Analysis of possible sources and acceleration mechanisms of ultra high energy cosmic rays

from
Sarah Schmetkamp

Bachelor thesis in physics

submitted to
Department of Mathematics, Informatics and Sciences
of
RWTH Aachen

in September 2009

produced at
Institute IIIb

under the supervision of
Prof. Dr. Hebbeker

Ich versichere, dass ich die Arbeit selbstständig verfasst und keine anderen als die angegebenen Quellen und Hilfsmittel benutzt sowie Zitate kenntlich gemacht habe.

Aachen, 24. September 2009

Contents

1 Introduction

In 1912 V. Hess performed a balloon flight measuring the electrical conductivity at different altitudes. He observed that it increases coming into higher regions of atmosphere and explained it by the ionizing effect of high-energy radiation from space (today called cosmic rays). In 1930 cosmic rays were identified to consist mainly of positive charged particles.[3]

Step by step the understanding of cosmic rays with energies from low to moderate energies (some 100 MeV to TeV) progressed. They can be accelerated within our galaxy, e.g. by magnetic fields of the sun. But the origins and the acceleration mechanisms of the ultra high energy cosmic rays are still unknown. The Pierre Auger Observatory started taking data in 2004 to gather more information about these cosmic rays with extreme high energies and gain a better understanding of the universe. [5][11]

Based on the work of the Pierre Auger Observatory current information of cosmic rays will be shown in this work followed by a section of different possible sources and acceleration mechanisms. Finally their relevance on the appearance of ultra high energy cosmic rays will be discussed.

2 Pierre Auger Observatory

In 1992 Jim Cronin and Alan Watson made first plans to build the Pierre Auger Observatory and to gain a better understanding of the ultra high energy cosmic rays by using extensive air showers.[32]

Since 2000 the observatory is constructed near Malargüe in western Argentina close to the Andes. Cosmic rays above 10^{19} eV have an estimated arrival rate of only 1 particle per square kilometre per year and the cosmic rays above 10^{20} eV, which are even more interesting, of just 1 per square kilometre per century. Therefore, the observatory covers an area of $3\,000\,\mathrm{km}^2$, which is roughly the size of Luxembourg, to have 30 events per year on average. In this area 1 600 surface detectors are placed separated 1.5 km from each other in a hexagonal structure. The Auger Observatory uses an hybrid technology, i.e. that additionally four stations, each including six fluorescence telescopes, are placed on the periphery of the instrumented area.[11] In figure 1 the layout is shown. The dots show the positions of the surface detectors, the green lines define the fields of view of the fluorescence telescopes. In the blue shaded area the detectors are already installed. The detectors outside this area are not placed yet.[4]

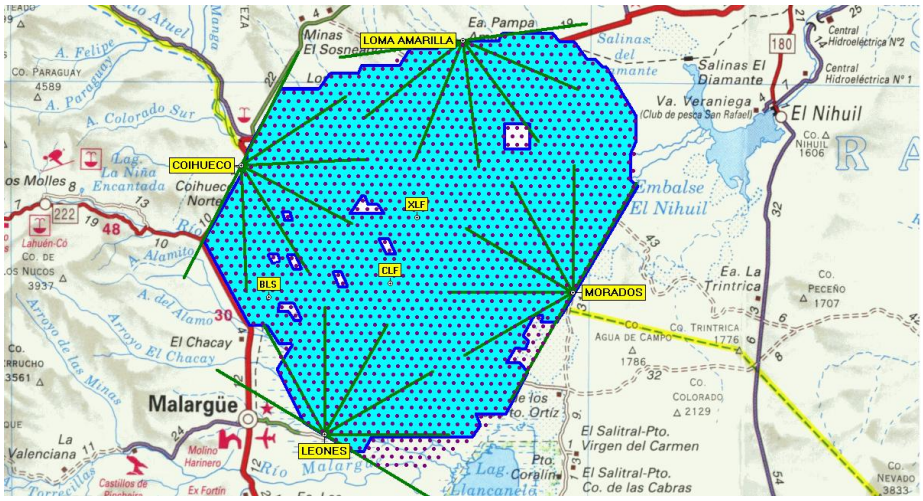

Figure 1: Layout of the Pierre Auger Observatory. The blue shaded area shows where detectors are already installed. The dots mark the positions of the surface detectors while the green lines define the fields of view for the fluorescence telescopes.[5]

In future another observatory will be built in south-eastern Colorado, USA, so that the northern hemisphere can be observed as well. This will lead to the ability of studying cosmic rays all over the sky.[10][9]

2.1 Detectors

As explained above the Pierre Auger Observatory uses a hybrid technology to measure air showers. These can be detected by both surface detectors and fluorescence telescopes. While the fluorescence telescopes can only work in clear and moonless nights (13% duty cycle), the surface detectors collect data continuously. This produces much more data from the surface detectors, but nevertheless the hybrid technology makes it possible to minimise the uncertainty of the measurement, e.g. by calibrating the energy measurement of the surface detectors with the fluorescence telescopes, since the error for the fluorescence telescopes is smaller than for the surface detectors.[11] Below the operating mode of the detectors will be described in more detail.

2.1.1 Surface Detector

Charged particles emit Cherenkov light if they move faster through a medium than the velocity of light in this medium, i.e. $v > \frac{c_0}{n}$, where v is the velocity of the particle, c_0 the speed of light in a vacuum and n the index of refraction. An electromagnetic shock wave, which is emitted at an angle of $cos(\Theta_c) = \frac{1}{n\beta}$, $\beta = \frac{v}{c}$, is created in the same way as a supersonic aircraft creates a sonic shock wave.[23]

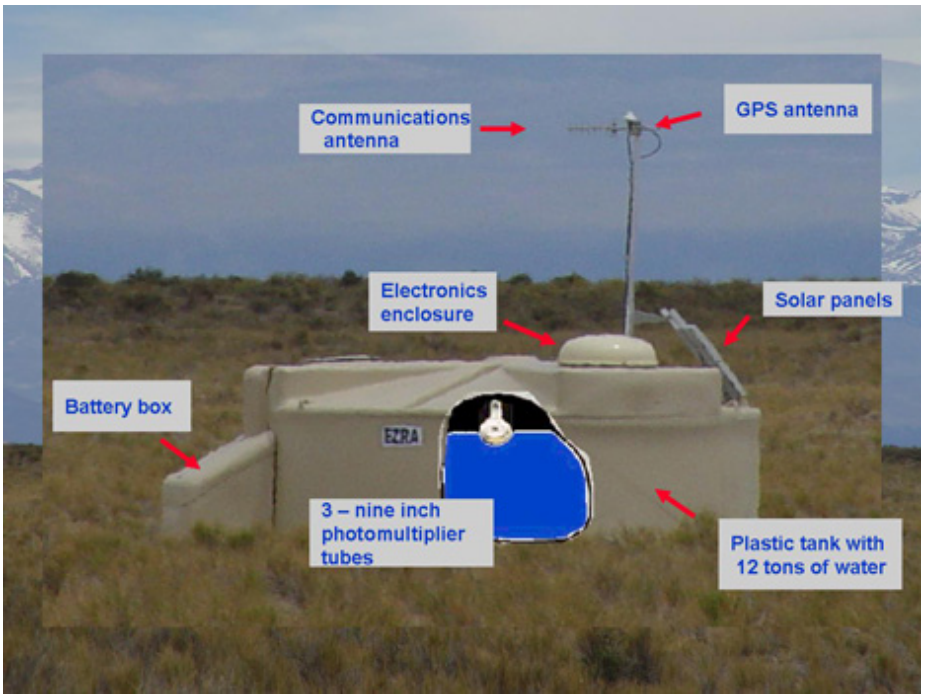

Figure 2: The surface detector is a plastic tank filled with 12 t of water. Photomultiplier are used to detect the Cherenkov light produced by the particles that move through the tank. The antenna is used to send the signal and its position to the main campus. The solar panels charge the battery which powers the electronics. [9]

The Pierre Auger Observatory utilises this light to detect the particles of the air showers and to measure the energy loss in the surface detectors. The surface detectors (see fig.2) are placed all over the detection area with a distance of 1.5 km to each other. Each station consists of a cylindrical tank with a base of 10 m^2 and a height of 1.2 m filled with 12 t of ultra pure water which serves as detection medium. The tanks are absolutely dark inside, so that the Cherenkov light emitted by the crossing particles can be seen. The light is reflected at the inside wall of the tank so that three nine inch photomultipliers on the surface of the water can measure it. Every 25 ns the signal is converted into an electrical signal inside a dome on the top of the tank which is send to the main campus via an antenna using a modified mobile communications network. In this way a measurement of deposited energy, arrival time and chronological sequence by the use of a GPS device is possible. The detectors are powered by solar panels which charge the batteries.[9]

An example of an event can be seen in figure 3. The dots represent the detector stations while grey means no signal and the signal strength increases from green to red. The ellipses mark the regions where the signals have the same strength. The arrow gives the arrival direction of the shower.

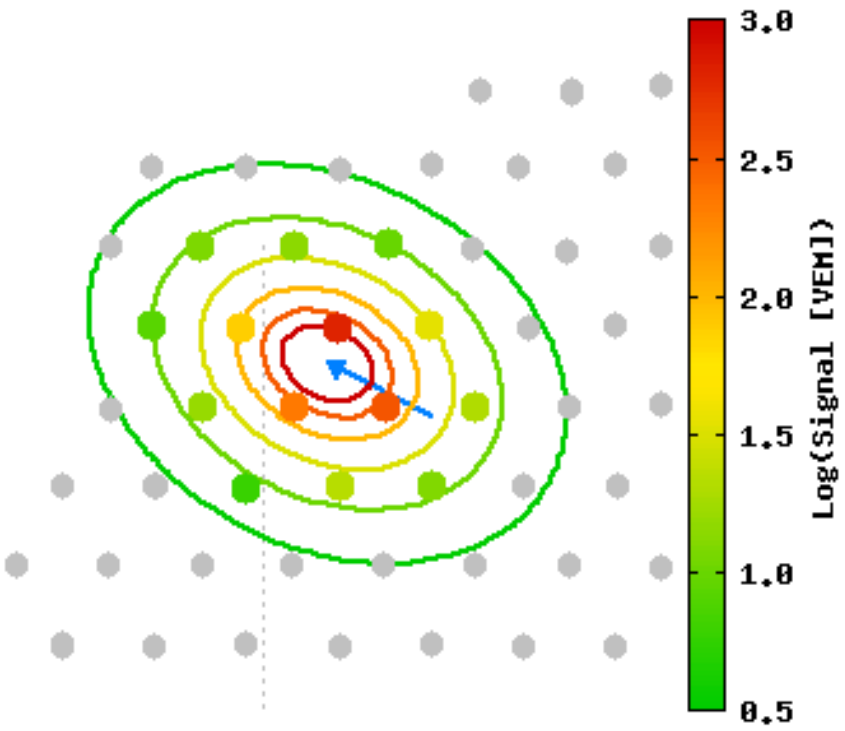

Figure 3: Signal of surface detector. The dots represent the surface detector stations, whereas their colour gives information about the signal strength. The ellipses show regions where the signals have the same strength and the arrow demonstrates the arrival direction of the shower.[6]

2.1.2 Fluorescence Telescope

Charged particles of the shower are able to excite nitrogen atoms in the air which will emit ultraviolet fluorescence light.

This light can be detected by the telescopes so the evolution of the shower can be seen on its full length. Each fluorescence telescope consists of a mirror with an area of $12\,\mathrm{m}^2$ which focuses the light to a camera containing 440 photomultipliers. This data is saved each $0.1\,\mu\mathrm{s}$. It can be used to identify the arrival direction, X_{max}, a shower parameter connected with the altitude where the shower has its maximum, and the energy of the primary particle.[7]

A typical signal is shown in figure 4. The viewing angle is plotted against the azimuth angle. The colour gives information about the time of detection whereupon blue corresponds to an early and red to a late one.

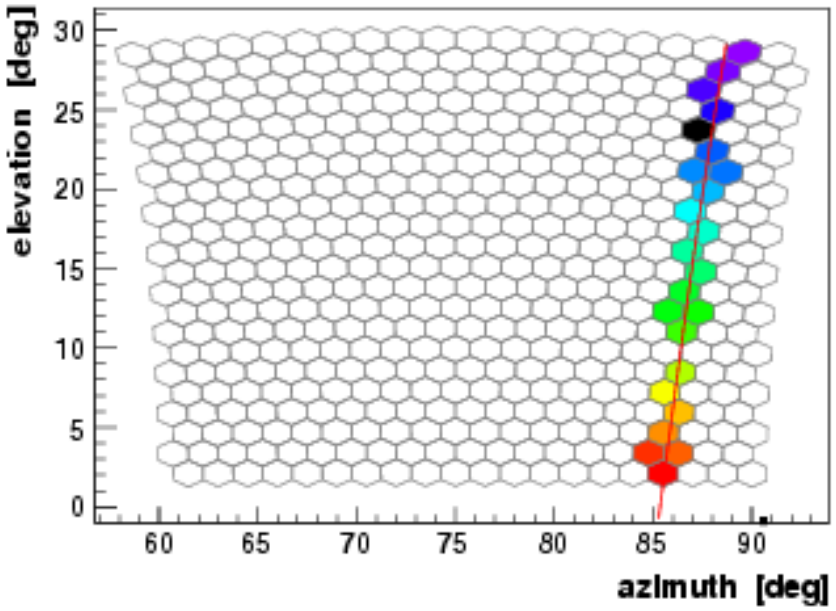

Figure 4: Signal of fluorescence telescope. Elevation is plotted against the azimuth angle. The colour shows the time signal(blue=early, red=late).[5]

2.2 Results

In the next sections the main results of the Auger Observatory will be presented. Looking at this results it becomes clear why the analysis of possible sources and acceleration mechanisms is important.

2.2.1 Energy Spectrum

The hybrid technology allows a calibration of the energy scale of the surface detectors by using the data from the fluorescence telescopes, since the error on the energy is smaller. In this way it is possible to measure the spectrum of energy with a higher precision due to higher statistics.

In figure 5 the resulting particle flux estimated with E^3 versus the energy is shown. It gives a hint on the GZK-cut-off, but this can only be verified if other reasons for this feature are excluded. By the analysis of composition and anisotropy one can find other motivations for the cut-off, e.g. a decreasing of the strength of the acceleration mechanism.[8]

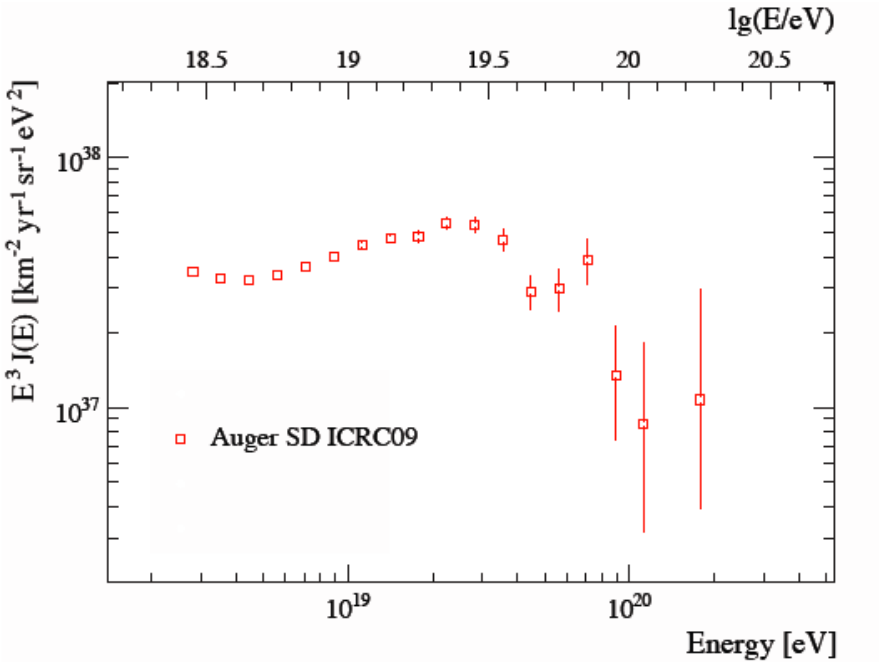

Figure 5: Energy spectrum measured by surface detectors. The flux is plotted versus the energy. It gives a hint on the GZK-cut-off.[38]

GZK-Cut-Off In 1966 the physicists K. Greisen, G. Zatsepin and V. Kuzmin predicted a cut-off in the energy spectrum at $6 \cdot 10^{19}$ eV. High energy protons ($E > 60$ EeV) are able to interact with the cosmic microwave background:

$$p + \gamma \rightarrow \Delta^+ \rightarrow \pi^0 + p \quad (1)$$
$$p + \gamma \rightarrow \Delta^+ \rightarrow \pi^+ + n \quad (2)$$

The Δ^+ has a short life time of only 10^{-23} s. If it decays into a proton and a pion, the proton can again interact with the cosmic microwave background until its energy falls below the 60 EeV threshold. Protons loose about 20% of their energy each time they interact.[22] Thus, the sources have to be closer than 100 Mpc, since otherwise they would have lost their energy by interacting with the cosmic microwave background.[20]

2.2.2 Composition

In figure 6 the composition of the ultra high energy cosmic rays(UHECR) is shown. The ordinate is labelled with X_{max} which is a shower parameter characterising the altitude of the shower maximum, that is correlated with the mass of the primary particle. The abscissa shows the energy. The coloured lines show the predictions of different interaction models if the cosmic rays are only consisting of iron or protons respectively. The plot shows three different data sets. In the one of the ICRC 2007 X_{max} was measured directly with the fluorescence

telescopes, while in the other cases indirect estimators from the surface detectors were used. All three sets show the same behaviour, namely the cosmic rays are consisting of different nuclei, whereas the composition is getting heavier at higher energies.[45]

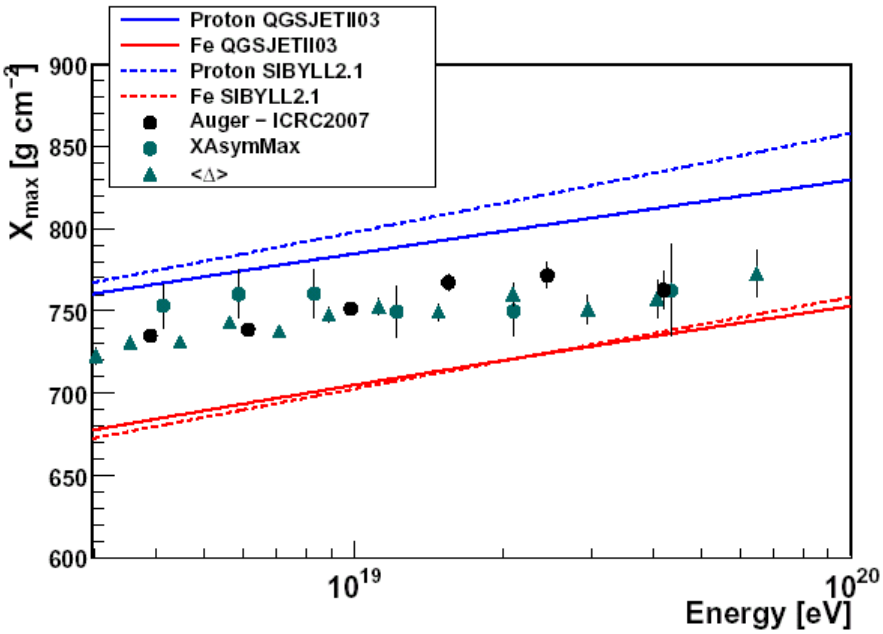

Figure 6: Composition of ultra high energy cosmic rays. The shower parameter X_{max} is plotted versus the energy. The coloured lines present predictions for the case of pure iron or pure protons respectively.[45]

2.2.3 Anisotropy

It is known that active galactic nuclei (AGN) are distributed anisotropically in our neighbourhood ($d < 200\,\mathrm{Mpc}$).[36] Therefore, it is an easy way to check if the arrival directions of cosmic rays show an anisotropic behaviour by discovering a correlation with the positions of AGN.

The result can be seen in figure 7. Whereas the blue area marks the sky which can be observed by the Auger Observatory (the more shaded the higher is the exposure). The red asterisks show the positions of AGN from the 12th edition of the Veron-Cetty and Veron catalogue under the cut parameter $z < 0.018$. The ellipses represent the arrival direction of the cosmic rays with $E > 57\,\mathrm{EeV}$ including the region of $3.1\,^{\circ}$.[4]

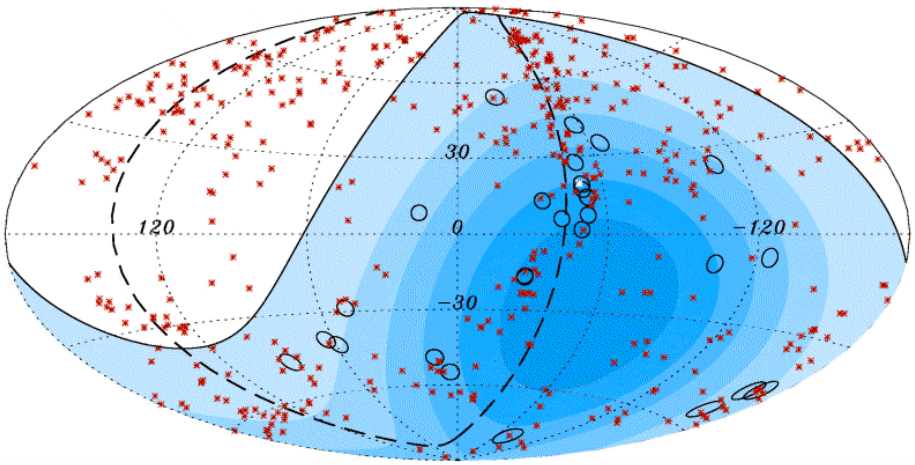

Figure 7: Correlation between AGN and arrival direction of ultra high energy cosmic rays. The shaded area shows the sky which can be observed by the Auger Observatory where a darker colour means a higher exposure. The asterisks mark the positions of AGN from the Veron-Cetty Veron catalogue with $z < 0.018$. The ellipses demonstrate the arrival directions of the cosmic rays including a region of 3.1 °.[4]

The observed correlation supported the hypothesis that ultra high energy cosmic rays have their origin in nearby extragalactic sources whose flux has not been reduced significantly by interactions with the cosmic microwave background. AGN or objects with similar spatial distributions are possible candidates for sources of ultra high energy cosmic rays. Some of them will be analysed in the next sections.[4][40]

3 Possible Sources

Leaving the precise acceleration mechanism aside Hillas gave an argument to identify objects which could be sources of ultra high energy cosmic rays.[33] In this section different possible sources of ultra high energy cosmic rays on the base of Hillas argumentation will be presented. First there will be a description of the particular candidate showing special properties. Later on it will be considered how far the different AGN types can be used as sources for ultra high energy cosmic rays.

Hillas Plot Hillas developed a simple dimensional argument which makes it possible to identify objects which are able to accelerate particles up to a given energy. The magnetic field (B) which keeps the particles in contact with the acceleration site and the size (R) of the acceleration region which has to be larger than the diameter of the orbit of the particle are main aspects. Taking into account the effect of the characteristic velocity βc of the magnetic scattering centres the following condition is the result:

$$\left(\frac{B}{\mu G}\right)\left(\frac{R}{kpc}\right) > 2\left(\frac{E}{10^{18}\,eV}\right)\frac{1}{Z\beta}. \tag{3}$$

The argument expressed by this equation is presented descriptive by the Hillas plot (see fig.8). Plotting the magnetic field against the size of the acceleration region it becomes clear that either a large magnetic field or a large size of the acceleration region is needed to achieve the given maximum energy. In case of an acceleration up to 10^{20} eV which is plotted here among others active galactic nuclei are possible sources.[33]

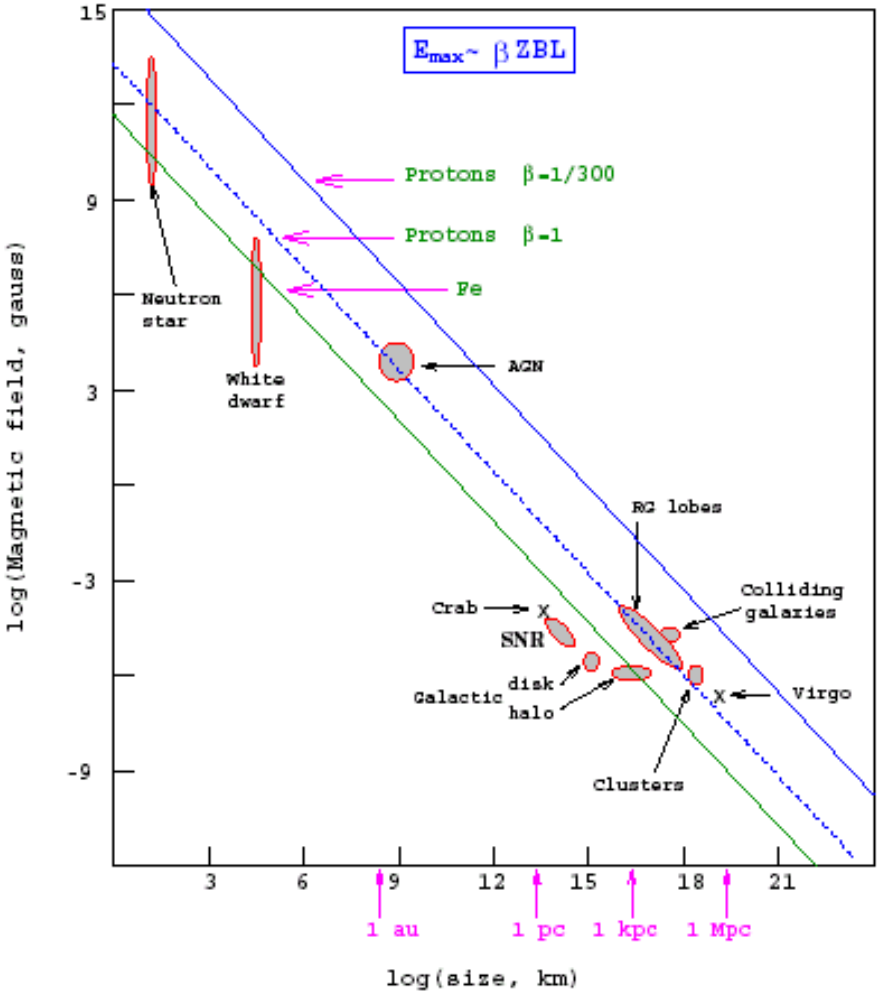

Figure 8: The Hillas plot is a presentation of the connection between the magnetic field (ordinate) and the size of the acceleration region (abscissa). Objects located in the area below the lines are not able to accelerate protons or iron respectively to the given energy.[33]

3.1 Active Galactic Nuclei

The bright inner part of particular host galaxies like spiral galaxies or elliptical galaxies is called Active Galactic Nuclei (AGN). There are some fundamental parts which are more or less distinctive in connection to each AGN (see fig.9):

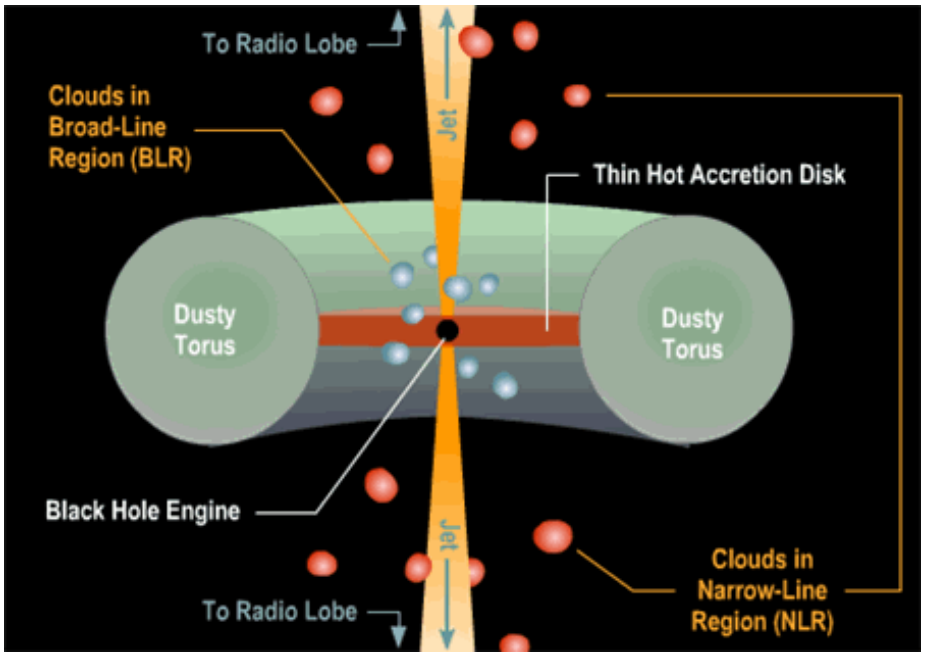

Figure 9: Schematic view of different parts of AGN. The dusty torus moves into the direction of the black hole becoming a thin accretion disk. Just before reaching the black hole matter is ejected in jets. Clouds with different velocities are located above and below the accretion disk. They change the optical properties of the emitted light.[15]

Many giant stars emit dust into their environment. This dust is located at the pc to kpc scale of the AGN rotating around it and building up an enormous toroidal reservoir of matter, the **Dusty Torus**. Depending on the orientation to the observer the Dusty Torus opens the view into the centre of the AGN (small inclination) or obstructs it (high inclination). This leads to a dichotomy of AGN into Type I AGN for small inclination and Type II AGN for high inclination.[29]

With decreasing distance to the black hole the temperature increases following the model of Shakura and Sunyaev[30] in which $T \propto r^{-\frac{3}{4}}$. Thermal energy is nearly completely emitted in form of radiation energy. Due to this and the rotation of the matter moving into the direction of the black hole following Kepler´s law the matter arranges in a flat form, named accretion disk, which is optical thick. Near the black hole the thermal energy is not emitted in form of radiation energy any more so the temperature becomes higher. Because of this higher temperature the accretion disk becomes toroidal again at the inner edge.[25]

Above the accretion disk we find a region where ionized clouds move with velocities of $(1,000-10,000)\,\frac{km}{s}$, called **Broad Line Region**, since the characteristic emission lines sent by this luminous moving matter are highly broadened due to the Doppler effect.[26] Further away these ionized clouds move only with velocities of $100\,\frac{km}{s}$, i.e. the emission lines are less broadened, we call this region the **Narrow Line Region**. Depending on the presence or absence of the broad emission lines AGN are classified into Type I or Type II which is of

course connected to the angle between the rotation axis and the direction of our observation.

In the centre of AGN a **Super Massive Black Hole** is located. Matter from the accretion disk falls into the black hole.[29] The gravitational energy is mainly dissipated into rotational energy which is dissipated again into thermal energy because of turbulences and shearing mechanisms. Finally the thermal energy is dissipated into radiation energy.[25] Even before reaching the event horizon the radiation process gets so strong that the AGN gains its characteristic luminosity.

Close to the super massive black hole plasma is ejected to distances up to several Mpc perpendicular to the accretion disk. Mainly by the effect of Lorentz force the matter is collimated into a **Jet**. At the end of it, where the plasma hits the interstellar medium hot regions occur, called Hot Spots.[29]

AGN can be classified with respect to many different properties like spectral or morphological differences. Many of them are shared by a number of different types but they can be distinguished more or less by other properties. The most important types of AGN will be described below and at the end of the section a table compares their most important properties.

3.1.1 Quasars

The most luminous AGN type is given by a Quasar. It is the generic term for quasi stellar objects which are radio quiet and quasi stellar radio sources which are radio loud. The highly red shifted spectrum of the Quasars gives a hint that they are extragalactic objects with distances of some Mpc to several hundred Mpc. Although Quasars can occur in every type of galaxy most of them are found in elliptical galaxies. About 90 % of all Quasars can be attached to Type I AGN whereas only 10 % are in Type II AGN. It turned out that the fraction of Type II AGN decreases by increasing luminosity. This leads to the assumption that the geometrical effect is not the only one which accounts the origin of both types. A possible explanation could be that the strong radiation pressure of very bright Quasars blows away the dusty torus and thus leads to a Type I. Radio quiet Quasars which seem to be more numerous than radio loud ones appear to have a spectrum similar to that of Seyfert galaxies showing broad emission lines, weak absorption lines, if at all, and powerful ultraviolet and X-ray emission, however, the activity of Quasars is stronger. Radio loud Quasars have a morphology similar to that of radio galaxies differing only by the smaller scale. In many Quasars radio jets only can be detected at one side of the nucleus.

Blazars A subclass of quasars which only occurs in elliptical galaxies is called Blazar. Blazars possess distinctive jets which are adjusted more or less into the direction of the observer. That is the reason why often only one jet can be detected. The Blazars emit γ-radiation up to energies of TeV which is even higher than for Quasars.

3.1.2 Seyfert Galaxies

Seyfert galaxies, named after their explorer Carl K. Seyfert, are lower-luminosity members of AGN. They mainly occur in spiral galaxies. The spectrum is similar to that of Quasars but with less activity. The emission lines are similar to those of low ionisation nuclear emission line regions (see below) regarding the width but with less power. Their jets are also less distinctive than in the case of Quasars and radio galaxies.

3.1.3 Radio Galaxies

Radio galaxies are radio loud objects with small luminosity. Most radio emission is send from radio lobes far outside the galaxy linked to the nucleus by jets, therefore all radio galaxies have strong jets. The morphology is similar to that of Quasars but on larger scales. Radio galaxies are elliptical or elliptical-like. They can be divided into Type I and Type II because of their emission spectrum and therefore can be seen as radio loud Seyfert galaxies. Additionally high-z radio galaxies can be found. The large red shift allows the analysis of jets in the early Universe which differ from those emitted recently.

3.1.4 Low Ionisation Nuclear Emission Line Regions

The most common type of AGN is the low ionisation nuclear emission line region (LINER). In this case the emitting region within the nucleus is low ionized. LINERs are located mainly in spiral galaxies, nearly 50% of all spiral galaxies contain detectable LINERs, but every early type galaxy may be a host galaxy. LINERs have a small luminosity with a spectrum which is very similar to that of Type II Seyfert galaxies. It shows weak broad emission lines, whereas also narrow ones can be seen. LINERs also emit radio synchrotron radiation which is similar to that of radio galaxies, but with less intensity.

3.1.5 BL Lac Objects

The name of this further type of AGN is derived from the first discovery of a BL Lac Object in the constellation of Lacerta which was classified to be a variable star and following the convention to name variable stars with alphabetic ongoing indices it was called BL. Long time later it was found out that these objects were only looking star-like but are extragalactic. BL Lac Objects occur in elliptical galaxies. This is supported by the absence of emission and absorption lines which is a sign of a missing gas disk and typical for this type of galaxies. The jet is pointing directly into the observers direction.

3.1.6 Ultra Luminous Infra Red Galaxies

Ultra Luminous Infra Red Galaxies (ULIRGs) are identified by their extreme luminosity in the infra red region, whereas they also show activity in the X-ray region. They occur in the same order of magnitude as the Seyfert galaxies and are even more common than Quasars. Powered by both star burst and AGN they can be regarded as a type of AGN.[29][34]

Type	Host Galaxy	Inclination	Spectrum
Quasar	all (elliptical)	Type I and II	IR, UV, X-ray, (radio)
Blazar	elliptical	small	γ
Seyfert	spiral	Type I and II	IR, UV, X-ray
Radio	elliptical	Type I and II	radio
LINER	spiral (all early)	high	radio, narrow emission lines
BL Lac	elliptical	very small	optical, radio, IR no emission/absorption lines
ULIRG	all	high	IR, X-ray

Table 1: Comparison of the most important properties of the AGN types described above

3.1.7 Estimation of reachable energies

Now it will be discussed which energies can be reached by particles accelerated in different regions of an AGN.

For the central regions of AGN R and B can be estimated to be

$$B \approx 0.02\,pc \tag{4}$$

$$and \quad R \approx 5\,G. \tag{5}$$

[33] Using the formula by Hillas (eq.3) this values lead to an energy in the order of 10^{19} eV for protons and 10^{20} eV for iron. So the centre of AGN is unlikely to be source of cosmic rays with energies above 10^{20} eV but could be the origin for cosmic rays up to some 10^{19} eV or 10^{20} eV respectively.

But there are important effects, which influence the reachable energy: the energy loss due to synchrotron and Compton processes and the energy gain due to acceleration. Taking these processes into their calculation Norman et al [14] came to the result that neither protons nor heavy nuclei can escape from the central region with energies above some 10^{16} eV.

There are some more suggestions [19][2][18][12] which try to explain the highest energies for protons or heavy nuclei if they escape from the centre of AGN, but all of them lead to the same result, that the central regions of AGN are unlikely to be sources of the ultra high energy cosmic rays.

To avoid this problem the acceleration site is located outside the centre. Interesting regions which hold this idea are the hot spots of radio galaxies. Because of the small density of photons in this region the energy loss due to photo-pion production is not significant. However, the magnetic field is the most uncertain parameter. Taking ideal values for the magnetic field strength maximised energies of up to 10^{21} eV are possible. So these regions could serve as sources for cosmic rays with energies above 10^{20} eV.

Using the radio galaxies that correlate with the arrival directions of the high energy cosmic rays another problem occurs. Most of these galaxies have distances > 100 Mpc from Earth,[33] i.e. that the GZK effect would prevent particles from reaching the Earth with such high energies even if they had had them at the source. However radio galaxies with less distances, e.g. Cen A, are good candidates to accelerate particles up to highest energies.

3.2 Pulsars

Pulsars are rotating neutron stars with strong magnetic fields (see fig.10). The magnetic field produces a jet of electromagnetic radiation which is send at the axis of the magnetic field. If this axis is inclined to the axis of rotation a pulsating signal is observed at Earth.[21]

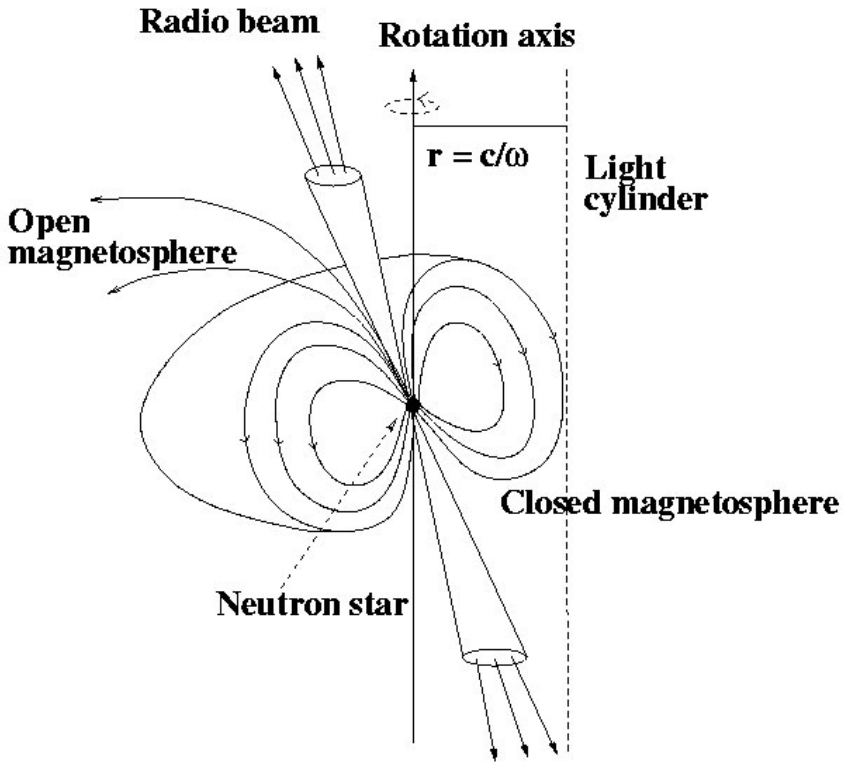

Figure 10: Schematic view of a pulsar. The axis of the magnetic field is inclined to the axis of rotation. At the axis of the magnetic field jets of electromagnetic radiation are ejected.[27]

Pulsars are galactic objects. Therefore they occur mainly within the galactic plain. At the moment about 1700 pulsars are known.[27]

In the following the origin of pulsars will be described explaining their properties.

Neutron stars result from very massive stars. The lifetime of stars is limited by their mass. The fusion of hydrogen and helium in the inner produces enough pressure to stop the collapse caused by gravitational force. In the case of massive stars fusion goes on until the nucleus consists of iron which is the end of fusion processes where energy can be obtained. The nucleus region collapses squeezing the atoms together if the mass of the nucleus is in the order of $1.9\,M_\odot \leq M \leq 2.5\,M_\odot$, where $M_\odot$ is the mass of the sun. A recombination producing neutrons and neutrinos starts:

$$e^- + p \rightarrow n + \nu_e \tag{6}$$

The collapse creates a shock wave ejecting the matter from the outer regions. The star explodes in a supernova leaving a neutron star.[21]

As a result of the collapse neutron stars have a radius of only $(10 - 15)\,\mathrm{km}$ and are very dense with $\rho = 10^{14}\,\frac{g}{cm^3}$. The gravitational force is 10^{11} times stronger than on the ground of the Earth. Neutron stars rotate faster than the origin stars due to the conservation of angular momentum and the downsizing in diameter. The frequence of rotation is in the order of 1 ms. Additionally the conservation of flux causes a magnetic field which is $10^6 - 10^8$ times stronger than before.[31] The absolute value of the magnetic field is between 10^8 G and 10^{12} G.[21]

Because of their strong magnetic fields and their high rotational frequency pulsars build up strong electrical fields. These can be used to accelerate particles directly.

Acceleration in pulsars is possible up to energies of $10^{21}\,\mathrm{eV}$ in principle. In reality the potential drop along the magnetic field lines which is causing the acceleration is short-circuited due to electrons and positrons which move in opposite directions along the magnetic field lines and interact with each other taking energy out of the system. Therefore acceleration of particles to energies above $10^{15}\,\mathrm{eV}$ in isolated neutron stars is hard to get.[33] Some other calculations based on accretion disk models [44][43] were made but they are not able to accelerate particles to higher energies.

Magnetars which are pulsars with even higher magnetic fields of up to 10^{15} G have more energy for the acceleration of particles but it is not sure if the problems due to the energy loss processes can be avoided.[33]

It was suggested that relativistic magnetohydrodynamic winds could accelerate iron ions to energies above $10^{20}\,\mathrm{eV}$[1], these could reach Earth without much energy loss. The composition should be highly dominated by iron in this case, but that is not supported by the date of the Auger Observatory.

There is some evidence that supernova remnants could be possible sources, so they will be analysed here as well.

3.3 Supernova Remnants

As explained above at the end of the life of a massive star a supernova takes place. The nucleus region collapses and creates a shock wave ejecting the matter from the outer regions. The shock wave of ejected matter is called supernova remnant (SNR).[21] At the beginning it moves with a velocity of $10,000\,\frac{km}{s}$ but this decreases continuously and after 10^6 a and at a dimension of 100 pc the SNR disintegrates moving now with the same velocity as the interstellar medium.[3]

Unless the acceleration mechanism works very efficient supernova remnants are not able to accelerate particles to energies above $10^{14}\,\mathrm{eV}$ since the size of the acceleration region is too small.[13]

3.4 Gamma Ray Bursts

Gamma ray bursts (GRBs) are very short (some ms to 100 s) radiation bursts of high energy γs. About one GRB is observed each day, distributed isotropically at the sky.[24] The number of γs which are produced by a single GRB is in the order of 10^{59}.[39] Depending of their duration GRBs can be divide into long and short ones.

Short GRBs last less than 2 s and result from the mergence of compact objects like neutron stars and black holes. Energies of $(10^{59} - 10^{61})$ eV can be set free.

Long GRBs last longer than 2 s and occur whenever young massive stars collapse and explode in a supernova creating energies of $(10^{62} - 10^{64})$ eV.[24] The γ-emission is strongly focussed.[24] Months after the GRB a afterglow in form of a X-ray flash can be observed.[39] A more detailed description of the evolution will follow in context with the cannonball model.[24]

The acceleration takes place all along the way of the cannonball, $R \approx 180$ pc, until the energy is depleted. Typical magnetic fields in Cannonballs are $B \approx 3$ G. Using this data and the formula of Hillas (3) energies above 10^{21}eV can be reached.

4 Acceleration Mechanisms

In the next sections acceleration mechanisms which occur in connection with the sources mentioned above will be analysed.

4.1 Fermi Acceleration

The Fermi acceleration can be structured into two different types. Since the second order Fermi acceleration is basic for the first order acceleration it will be described here first.

4.1.1 Second Order Fermi Acceleration

The acceleration takes place e.g. in jets of AGN and shock waves of supernova remnants and is the fundament of most acceleration mechanisms. Particles diffusing through a plasma scatter off magnetic inhomogeneities.[28] The process is shown in figure 11

Regions of magnetised plasma, called magnetised clouds, move with velocities of about 15 $\frac{km}{s}$. If a particle enters the cloud it is scattered off the magnetic inhomogeneities. In case the cloud moves away the particle will loose energy in this process, otherwise it will gain energy. Because it is less often that clouds move away the particle gains energy in average. In the rest system of the cloud the scattering is collision less and the energy is constant. The direction of scatter and also the direction the particle leaves the cloud are distributed randomly. With that information the energy gain can be calculated to be

$$\frac{<\Delta E>}{E} = \frac{1 + \frac{\beta^2}{3}}{1 - \beta^2} \cong \frac{4}{3}\beta^2, \tag{7}$$

where E is the energy, $< \Delta E >$ is the mean energy difference and $\beta = \frac{v}{c}$. Because of the dependence of β^2 the gain of energy is very small.[35][41]

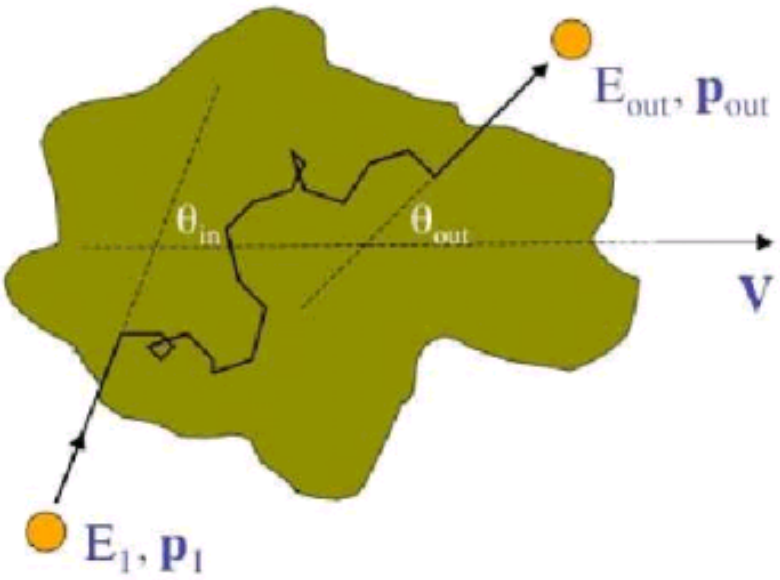

Figure 11: Acceleration at magnetised clouds - Fermi II. The particles are deflected by magnetic inhomogeneities and gain energy.[37]

4.1.2 First Order Fermi Acceleration

This type of acceleration works in the propagating plasma of shock waves, e.g. of supernova remnants. Its mechanism is demonstrated in figure 12 and will be described below.

If the shock front propagates with velocity U through the interstellar medium the plasma gets shocked and creates turbulent magnetic fields. In the rest system of the shock front the unshocked comes nearer with the velocity U while the shocked plasm moves away with $\frac{1}{4}U$ which can be calculated from thermodynamics.

In the rest system of a particle within the unshocked plasma which will be accelerated the shocked material moves towards it with velocity $\frac{3}{4}U$. Therefore the particle enters the shocked medium and is accelerated within the magnetic inhomogeneities on the mechanism of Fermi II until it gained so much energy that it can be regarded as a part of the shocked medium. Then the unshocked material moves towards the particle with $\frac{3}{4}U$ and the particle enters it. Again it is accelerated by the magnetic inhomogeneities on Fermi II mechanism.

This process leads to the conclusion that the particle will move through the shock front, and gain some energy each time, until the energy of the shock front is completely consumed. Then the particle, which now has ultra high energy, is set free and can be detected at Earth.[37]

The mean gain in energy for strong shocks is given by

$$\frac{< \Delta E >}{E} = \frac{1 + \frac{4\beta_{plasma}^2}{3} + \frac{4\beta_{plasma}^2}{9}}{1 - \beta_{plasma}^2 - 1} \cong \frac{4}{3}\beta_{plasma} \cong \beta_{shock}, \tag{8}$$

where E is the energy, $< \Delta E >$ is the mean energy difference and $\beta = \frac{v}{c}$. In this case the energy gain is linear in β_{shock}, i.e. it is stronger than for Fermi II.[41] Therefore, this acceleration mechanism is well suited to be accelerator of ultra high energy cosmic rays.

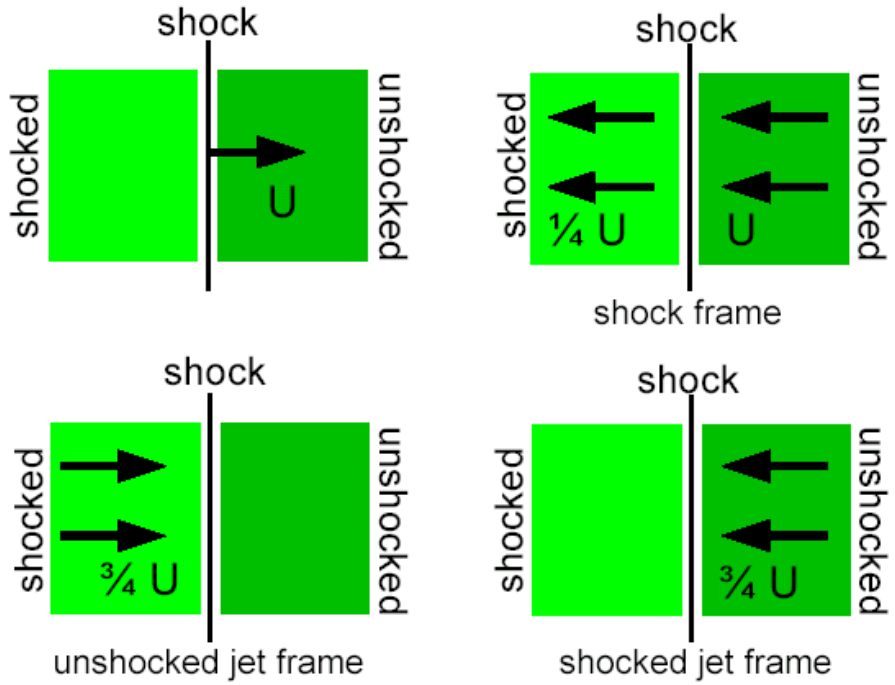

Figure 12: Acceleration at shock front - Fermi I. Independent of the position of the particle with regard to the shock front the shock front moves towards the particle in its rest system. It penetrates the shock front and is accelerated by magnetic inhomogeneities in the way of Fermi II acceleration. The accelerated particle is given into the environment if the shock front has lost its energy and disintegrates.[37]

4.2 Shear Acceleration

Shear accelleration occurs in powerful astrophysical jets. The acceleration takes place if energetic particles encounter a region with different local flow velocities. They scatter elastically off small scale inhomogeneities in the magnetic field and are accelerated.

In the co-moving flow frame where the electrical field vanishes the particle momentum is randomized in direction but the magnitude is conserved. The rest frame of the scattering centres is equal to that of the background flow. Therefore

the particles gain no energy or momentum in scattering processes if there is no shear and the flow is not diverging. The shear in the background flow makes the particle momentum change relative to the flow when travelling across the shear. Because in the local flow frame the particle momentum is preserved in subsequent scattering events the particle momentum increases.

There are three possible velocity shear sites:

- gradual velocity shear parallel to the jet axis and a velocity profile which is decreasing outward linearly
- gradual velocity shear perpendicular to the jet axis
- non gradual (discontinuous) longitudinal velocity shear at the jet side boundary

The gradual velocity shear parallel to the jet axis is caused by interactions between the jet and the ambient medium. Because the velocity changes continuously within the shear region and the mean free path is much smaller than the transverse scale of the shear region energetic particles experience a gradual shear profile. Jets are structured in layers of the same velocity, while inner ones are faster than outer ones. The acceleration works well for protons because synchrotron losses are not able to stop the acceleration once it works efficiently as it would be in the case of electrons. The acceleration of particles will go on until the particle escapes.

The gradual velocity shear perpendicular to the jet axis is caused by the intrinsic rotation of the jet. This substantial rotation is required for efficient acceleration. As described above the acceleration process can not be stopped by synchrotron losses once it works efficiently.

In case of the non gradual longitudinal velocity shear at the jet side boundary the mean free path is larger than the transversal width of the layer, i.e. the particle passes the jet unaffected experiencing a discontinuous drop in velocity. The acceleration is caused by the scatter of particles off magnetic inhomogeneities and works nearly all along the jet which makes it even more efficient.[16]

Unless the acceleration mechanism is efficient for protons more than for electrons, gradual shear flow is only able to accelerate protons up to 10^{19} eV. Non gradual shear acceleration is able to reach even higher energies, up to 10^{20} eV but that is not enough to explain the extreme high energy cosmic rays we observe.[17]

4.3 Cannonball Model

The cannonball model is an acceleration mechanism which takes place in connection with GRBs. It is able to explain the observation of long GRBs and to accelerate particles up to highest energies. A demonstration of the process is given in figure 13.

Cannonballs can be understood as a type of jets. About once a month two oppositely directed cannonballs are sent by the black hole caused by matter, e.g. from a supernova explosion, which is falling into the black hole.[39]

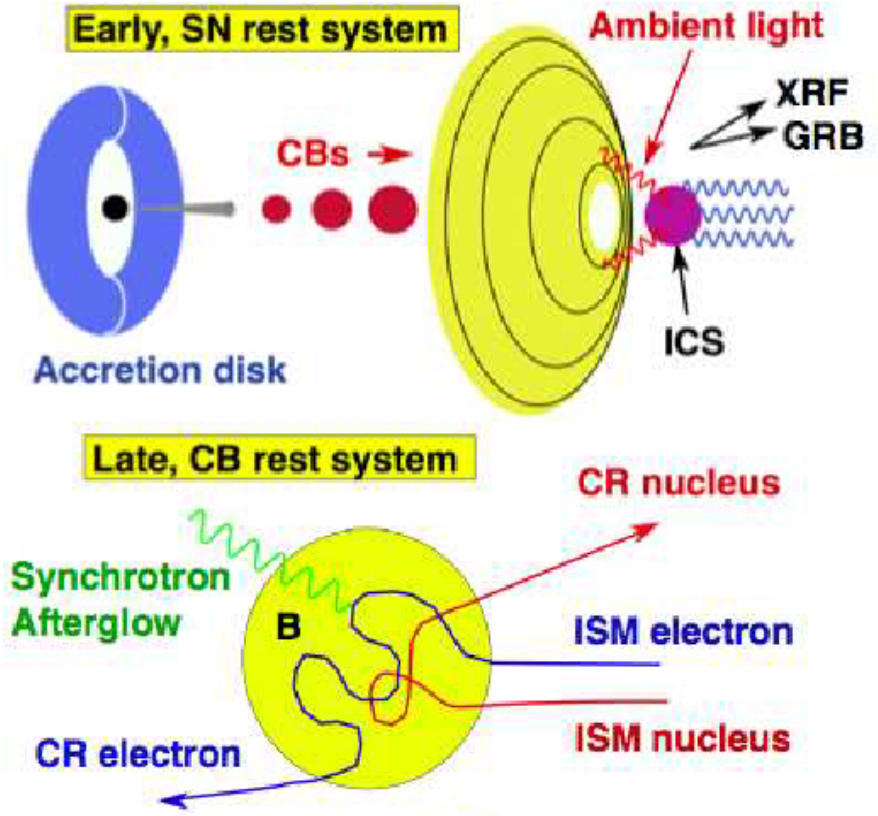

Figure 13: Cannonball model. A supernova leaves a black hole with an accretion disk around it. If matter from the accretion disk falls into the direction of the black hole it is ejected in cannonballs. At the moment the cannonball penetrates the shock front of the supernova remnant the ambient light interacts with the electrons within the cannonball (Inverse Compton scattering) and gains energy, the Gamma ray burst. Electrons and nuclei are deflected by magnetic inhomogeneities within the magnetic field. Nuclei gain energy and are accelerated whereas electrons emit synchrotron radiation which can be seen as the afterglow.[39]

If the cannonball penetrates the shock front of the supernova remnant the electrons within it start inverse Compton scattering with the ambient light. In this process the photons gain energy and are emitted within only small deflection into the direction of the cannonballs moving direction. Depending on the energy of the photons we distinguish between GRBs and X-ray flashes. On their way through the interstellar medium they ionise it.

Within the cannonball, which is moving through the ionised interstellar medium turbulent magnetic fields are created. If electrons and nuclei from the interstellar medium enter the cannonball they are deflected by the magnetic field due to Fermi II acceleration and become cosmic rays. Whereas the electrons loose some energy due to synchrotron radiation and therefore cannot

reach the highest energies, in contrast to multiple charged nuclei, which can be accelerated up to energies of 10^{21} eV[39]

5 Calculation Example

Under the assumption that the sources are distributed homogeneous and emit high energy cosmic rays in every direction in the same way it can be checked if different models which want to explain the origin of ultra high energy cosmic rays are able to explain the flux measured on Earth.

If there was only one source responsible for all cosmic rays it should account for all the flux. Therefore, the flux is in a distance r_s from the source

$$\Phi_s = \frac{\frac{dN_s}{dt}}{4\pi r_s^2}, \tag{9}$$

where Φ_s is the flux from one source and $\frac{dN_s}{dt}$ is the event rate. If we consider many sources it is necessary to integrate over the whole volume to get the overall flux. The source density is defined to be constant for a special type of sources. The GZK effect is considered by taking a constant value of 100 Mpc for the horizon and making a strict limit there. For a spherical-symmetrical detector the flux can be calculated by

$$\Phi_{all} = \int \Phi_s \rho_s dV = 4\pi \int_0^R \frac{\frac{dN_s}{dt}}{4\pi r_s^2} \rho_s r_s^2 dr_s = \frac{dN_s}{dt} \rho_s R. \tag{10}$$

In this analysis the flux has to be tested by using data from the Auger Observatory. The flux measured by Auger is multiplied by a factor of 4π to get the value of Φ_{All} since the Auger result is normalised to a sr. The equation can be transformed as follows:

$$\Phi_{All} = 4\pi \Phi_{Auger} = \frac{dN_s}{dt} \rho_s R \tag{11}$$

$$\rho_s = \frac{4\pi \Phi_{Auger}}{\frac{dN_s}{dt} R} \tag{12}$$

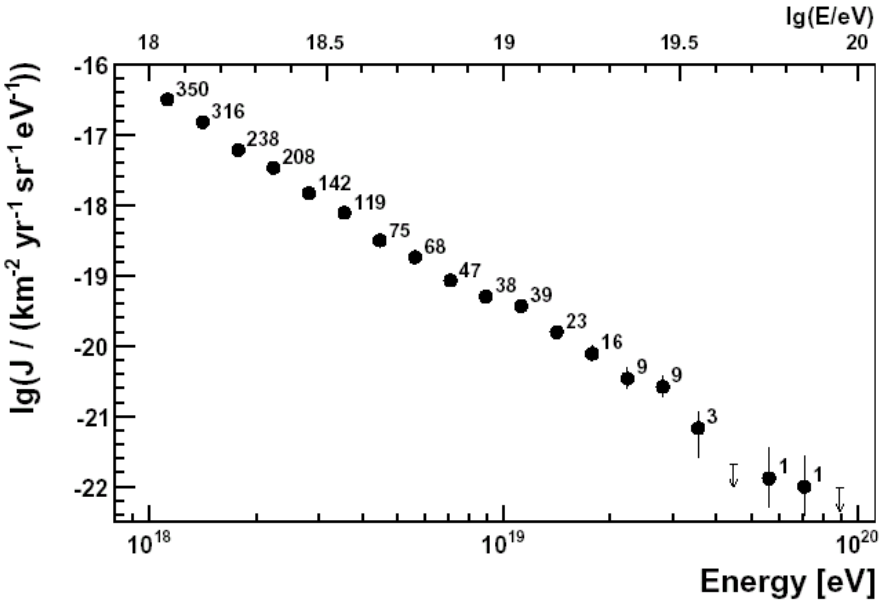

Figure 14: Energy spectrum measured by surface detectors of Auger Observatory.[42]

The flux measured by Auger can be taken out of figure 14 for a certain energy bin, i.e. the entry of that bin is multiplied by its width. For energies around 45 EeV it is $10^{26}\,\frac{1}{(Mpc)^2(yr)(sr)}$. By variation of N_s one gets the plot of figure 15.

Now several models can be tested. For example taking the source density of the AGN from the Veron-Cetty Veron catalogue, depending on the source model this is $((10^{-5}$ to $10^{-3})\frac{1}{(Mpc)^3})$, a value of $(10^{28}$ to $10^{30})\frac{1}{yr}$ for the number of particles appears.

This value can be compared with the number of photons which are emitted in a GRB. Using the total energy of a GRB of about 10^{63} eV and the energy of a single photon of about 1 TeV, it turns out that 10^{51} photons are emitted in each GRB. In contrast to that the number of particles calculated above seems to be small. To interpret the result correctly a more detailed analysis of the single models would be necessary, which could be done in further studies.

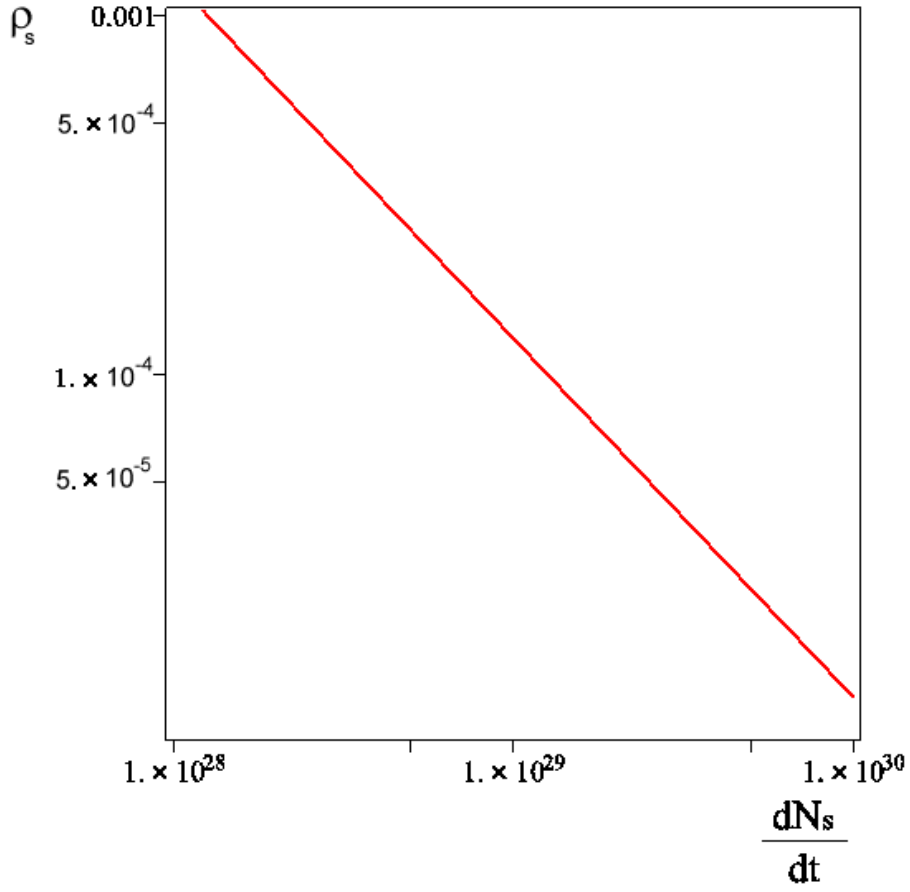

Figure 15: Source density vs event rate.

6 Conclusion

After having studied the different types of possible sources and acceleration mechanisms it turned out that the amount of different models is enormous but only some of them are able to explain the observations. At the moment it is not possible to make a sure statement of the processes which lead to the ultra high energy cosmic rays we are able to observe.

The results of the Pierre Auger Observatory are an important step towards the understanding of ultra high energy cosmic rays unless many questions are not answered yet and will need some more time of research.

From the sources I observed in my thesis AGN, in particular the hot spots, and GRB turned out to be well suited for acceleration of particles to ultra high energies. Second order Fermi acceleration is the fundament of nearly all acceleration mechanisms unless it is very inefficient on its own and can not reach high energies. First order Fermi acceleration and the cannonball model seem to be good candidates of acceleration.

In the table below the different possible sources and acceleration mechanisms I analysed are compared, showing the energies which can be gained.

Source	**Acceleration Mechanism**	**Reachable Energy (eV)**
Supernova	Fermi I	10^{14}
Pulsar	electric field	10^{15}
AGN	Fermi I	10^{21}
GRB	Cannonball	10^{21}

Table 2: Comparison of the efficiency of different sources and acceleration mechanisms.

References

[1] P. Blasi A. Olinto, R. Epstein. Galactic ultra-high-energy cosmic rays. 1999.

[2] R. Protheroe A. Szabo. Implications of particle acceleration in active galactic nuclei for cosmic rays and high-energy neutrino astronomy. *Astropart. Phys.*, 2:375–392, 1994.

[3] B. Baschek A. Unsoeld. *Der neue Kosmos, Einfuehrung in die Astronomie und Astrophysik*. Springer-Verlag, Berlin, 7th edition, 2005.

[4] J. Abraham et al. Correlation of the highest energy cosmic rays with nearby extragalactic objects. *Science*, 318:938–943, 2007.

[5] `http://www.auger.org/`. looked up at August, 1st 2009.

[6] `http://auger.colostate.edu/ED/`. number 1234800, looked up at August, 3rd 2009.

[7] `http://www.auger.de/public/fd.html`. looked up at August, 3rd 2009.

[8] `http://www.auger.de/public/fluss.html`. looked up at August, 7th 2009.

[9] `http://www.auger.org/features/inside_surface_detector.html`. looked up at August, 1st 2009.

[10] `http://www.auger.de/public/observatorium.html`. looked up at August, 1st 2009.

[11] `http://www.auger.org/observatory/`. looked up at August, 1st 2009.

[12] V. Berezinsky. *Nucl. Phys. B (Proc. Suppl.)*, 38:363, 1995.

[13] H. Besier. Die kosmische Strahlung und ihre Untersuchung im CosmoALEPH-Experiment, 2000. Staatsexamensarbeit Johannes Gutenberg-Universitaet Mainz.

[14] A. Achterberg C. Norman, D. Melrose. *Astrophys. J.*, 454:60, 1995.

[15] `http://www.astro.ufl.edu/circe/sci_agn.html`. looked up at July, 30th 2009.

[16] P. Duffy F. Rieger. Shear acceleration in relativistic astrophysical jets. *Astrophys. J.*, 617:155–161, 2004.

[17] P. Duffy F. Rieger, V. Bosch-Ramon. Fermi acceleration in astrophysical jets. *Astrophys. Space Sci.*, 309:119–125, 2007.

[18] M. Salamon F. Stecker. *Space. Sc. Rev.*, 75:341, 1996.

[19] M. Salamon P. Sommers F. Stecker, C. Done. *Phys. Rev. Lett.*, 66:2697, 1991.

[20] T.Porter C. Cheung I. Moskalenko, L. Stawarz. On the Possible Association of Ultra High Energy Cosmic Rays with Nearby Active Galaxies. *Astrophys. J.*, 693:1261–1274, 2009.

[21] B. Klein. Die Suche nach hochdispergierten Radio-Pulsaren in Richtung des Galaktischen Zentrums, 2005. Dissertation Bonn 2005 urn:nbn:de:hbz:5N-05369.

[22] M. Knoedlseder. Kosmische Strahlung, Energie und Zusammensetzung, December 2008.

[23] W. Leo. *Techniques for Nuclear and Particle Physics Experiments, A How-to Approach*. Springer-Verlag, New York, second edition, 1994.

[24] A. Mueller. `http://www.wissenschaft-online.de/astrowissen/lexdt_g.html#grb`. looked up at August, 11th 2009.

[25] A. Mueller. Lexikon der Astrophysik. `http://www.wissenschaft-online.de/astrowissen/lexdt_s07.html#ssd`. looked up at July, 30th 2009.

[26] A. Mueller. Lexikon der Astrophysik. `http://www.wissenschaft-online.de/astrowissen/lexdt_r04`. looked up at August, 12th 2009.

[27] A. Mueller. Lexikon der Astrophysik. `http://www.wissenschaft-online.de/astrowissen/lexdt_p08.html`. looked up at September, 12th 2009.

[28] A. Mueller. Lexikon der Astrophysik. `http://www.wissenschaft-online.de/astrowissen/lexdt_f02.html`. looked up at July, 13th 2009.

[29] A. Mueller. Aktive Galaktische Kerne - Leuchtfeuer im All, 2007.

[30] R. Sunyaev N. Shakura. Black Holes in Binary Systems. Observational Appearance. *Astron. and Astrophys.*, 24:337–355, 1973.

[31] P. Ostler. Pulsare, 2006. Presentation.

[32] `http://auger.cnrs.fr/pierre_auger.html`. looked up at August, 1st 2009.

[33] G. Sigl P. Bhattacharjee. Origin and propagation of extremely high energy cosmic rays. *Phys. Rept.*, 327:109–247, 2000.

[34] G. T. Petrov. `http://www.astro.bas.bg/~petrov/galaxies_files/agn.html`, 2004. looked up at July, 30th 2009.

[35] R. Protheroe. Origin and propagation of the highest energy cosmic rays. 1996.

[36] S. Sazonov E. Churazov R. Sunyaev R. Krivonos, M. Revnivtsev. `http://www.mpa-garching.mpg.de/mpa/research/current_research/hl2007-5/hl2007-5-de.html`. looked up at August, 18th 2009.

[37] G. Roper. Ausarbeitung zum Seminarvortrag ueber kosmische Strahlung, 2005.

[38] M. Roth. Measurement of the energy spectrum of cosmic rays from the Pierre Auger Observatory. `http://web.phys.ntnu.no/~mika/programme.html`, 2009. Presentation at SOCoR, Trondheim.

[39] A. De Rujula. An introduction to Cosmic Rays and Gamma-Ray Bursts, and to their simple understanding. 2007.

[40] S. Troitsky S. Gureev. Physical conditions in potential sources of ultra-high-energy cosmic rays. II. Nearby active galaxies correlated with Auger events. 2008.

[41] S. Menke S.Bethke. Kosmische Beschleuniger. Teilchenphysik mit kosmischen und erdgebundenen Beschleunigern. Presentation.

[42] F. Schuessler. Measurement of the cosmic ray energy spectrum above $10^{18} eV$ using the Pierre Auger Observatory. In *PROCEEDINGS OF THE 31st ICRC*. Pierre Auger Collaboration, 2009.

[43] F. Takahara. Particle acceleration mechanisms in astrophysics. In *Fukugita, M. (ed.), Suzuki, A. (ed.): Physics and astrophysics of neutrinos* 900-934.

[44] V. Berezinsky S. Bulanov V. Ptuskin V. Ginzburg, (ed.) V. Dogiel. Astrophysics of cosmic rays. Amsterdam, Netherlands: North-Holland (1990) 534 p.

[45] H. Wahlberg. Study of the nuclear mass composition of UHECR with the surface detectors of the Pierre Auger Observatory. In *Proceedings of the 31st ICRC*, pages 8–10. Pierre Auger Collaboration, 2009.